López et al. Journal of Neuroinflammation (2018) 15:158
https://doi.org/10.1186/s12974-018-1174-9

Journal of Neuroinflammation

RESEARCH Open Access

Cannabinoid CB_2 receptors in the mouse brain: relevance for Alzheimer's disease

Alicia López[1,2], Noelia Aparicio[1,3], M. Ruth Pazos[1,3], M. Teresa Grande[3], M. Asunción Barreda-Manso[1,3], Irene Benito-Cuesta[3], Carmen Vázquez[1], Mario Amores[1], Gonzalo Ruiz-Pérez[3], Elena García-García[1], Margaret Beatka[4,5], Rosa M. Tolón[1,3], Bonnie N. Dittel[4], Cecilia J. Hillard[5] and Julián Romero[1,3*]

Abstract

Background: Because of their low levels of expression and the inadequacy of current research tools, CB_2 cannabinoid receptors (CB_2R) have been difficult to study, particularly in the brain. This receptor is especially relevant in the context of neuroinflammation, so novel tools are needed to unveil its pathophysiological role(s).

Methods: We have generated a transgenic mouse model in which the expression of enhanced green fluorescent protein (EGFP) is under the control of the *cnr2* gene promoter through the insertion of an Internal Ribosomal Entry Site followed by the EGFP coding region immediately 3′ of the *cnr2* gene and crossed these mice with mice expressing five familial Alzheimer's disease (AD) mutations (5xFAD).

Results: Expression of EGFP in control mice was below the level of detection in all regions of the central nervous system (CNS) that we examined. CB_2R-dependent-EGFP expression was detected in the CNS of 3-month-old AD mice in areas of intense inflammation and amyloid deposition; expression was coincident with the appearance of plaques in the cortex, hippocampus, brain stem, and thalamus. The expression of EGFP increased as a function of plaque formation and subsequent microgliosis and was restricted to microglial cells located in close proximity to neuritic plaques. AD mice with CB_2R deletion exhibited decreased neuritic plaques with no changes in IL1β expression.

Conclusions: Using a novel reporter mouse line, we found no evidence for CB_2R expression in the healthy CNS but clear up-regulation in the context of amyloid-triggered neuroinflammation. Data from CB_2R null mice indicate that they play a complex role in the response to plaque formation.

Keywords: Cannabinoid CB_2 receptor, Transgenic mice, Enhanced green fluorescent protein, Amyloid, Neuroinflammation, Microglia

Background

It has been long appreciated that cannabinoids such as Δ^9-tetrahydrocannabinol (THC) exert effects on the immune system [40]. A primary target for the cannabinoids to alter immune system function, the cannabinoid receptor, subtype 2 (CB_2R), was identified molecularly in 1993 [23]. Autoradiographic and in situ hybridization studies indicated a high level of expression of the CB_2R in cellular elements of the immune system but these methods did not detect CB_2R expression in the central nervous system (CNS) [12, 18]. According to these early data, the abundance of CB_2R message in human blood cells was highest in B-lymphocytes, followed by natural killer cells, macrophages, and cluster of differentiation (CD)8 and CD4 T-lymphocytes [12].

The presence of CB_2Rs in the CNS has been the subject of intense debate during the last decade. Some reports [13, 35] showed the expression of CB_2Rs in neuronal elements of the uninjured brain, based primarily on immunohistochemical approaches. Other studies, however, limited the presence of CB_2R in the CNS to glial cells and, specifically, to microglia [6]. Seminal studies by Cabral and colleagues suggested that CB_2R could be expressed by microglial cells and that the expression level varied as a function of cell activation [9]. Subsequent studies

* Correspondence: j.romero.prof@ufv.es
[1]Laboratorio de Apoyo a la Investigación, Hospital Universitario Fundación Alcorcón, C/ Budapest 1, 28922 Alcorcón, Madrid, Spain
[3]Faculty of Experimental Sciences, Universidad Francisco de Vitoria, 28223 Pozuelo de Alarcón, Madrid, Spain
Full list of author information is available at the end of the article

confirmed this hypothesis [19, 31]. Regarding human samples, we found expression of CB_2R was restricted to perivascular microglia in control brains [24] but that CB_2R protein were dramatically increased in different pathological conditions. Observations made in Alzheimer's disease (AD), multiple sclerosis, Down's syndrome, and immunodeficiency virus-induced encephalitis confirmed that the presence of CB_2R is greatly enhanced in areas of neuroinflammation, predominantly in microglial cells (see [6], for a review).

However, concerns regarding the lack of specificity of antibodies against the CB_2R protein have been raised [3] (Additional file 1), which call into question some of these results. It is clear that additional tools are needed to unambiguously demonstrate the cellular expression of CB_2R throughout the body, but most particularly within the CNS. We here introduce a novel transgenic model designed to unveil the functional distribution of cannabinoid CB_2R and present data regarding the expression of these receptors in the mouse, with special attention to the CNS. Furthermore, we used this new mouse model to analyze the changes in the brain expression pattern of this receptor in the context of AD.

Methods

Generation of $CB_2^{EGFP/f/f}$ and $CB_2^{-/-}$ mice

Mice were generated at Genoway facilities (Lyon, France). A targeting strategy was designed consisting in the insertion of an enhanced Green Fluorescent Protein (EGFP) reporter gene, preceded by an Internal Ribosomal Entry Site (IRES) sequence in the 3′ untranslated region (UTR) of the *cnr2* mouse gene. This approach results in the expression of the reporter gene under the control of the endogenous mouse *cnr2* promoter and transcript from the same bicistronic mRNA as the CB_2R protein. Further, the entire exon 3, including the 3′ UTR and knocked-in reporter, is flanked by *lox*P sites, allowing the conditional inactivation of the *cnr2* gene in cells expressing Cre recombinase (Fig. 1a).

Three isolated sequences encompassing the murine *cnr2* gene regions surrounding the targeted exon 3 were used for the construction of the targeting vector. These sequences included (i) a 3462 bp-sized fragment

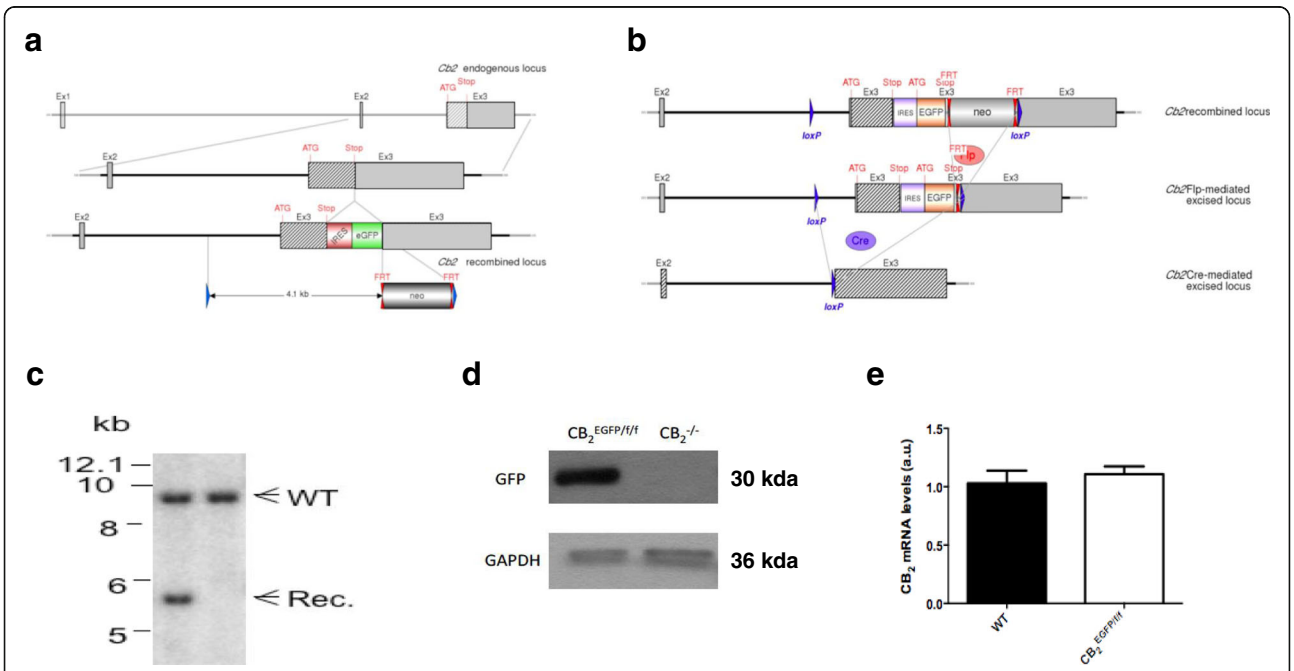

Fig. 1 Generation of a novel mouse model. **a** Genomic structure of the construct employed for the generation of $CB_2^{EGFP/f/f}$ and $CB_2^{-/-}$ mice. Hatched rectangles represent *cnr2* coding sequences, gray rectangles indicate non-coding exon portions, solid lines represent chromosome sequences. The neomycin-positive selection cassette (Neo) IRES sequence and reporter gene (EGFP) are indicated. *lox*P sites are represented by blue triangles and FRT sites by double red triangles. The initiation (ATG) and Stop (Stop) codons are indicated. For the generation of knock-in mice ($CB_2^{EGFP/f/f}$), recombined mice were bred with ubiquitous FLP-recombinase expressing mice, enabling the deletion of the FRT-flanked region. **b** For the generation of knock-out mice ($CB_2^{-/-}$), recombined mice were bred with ubiquitous Cre-recombinase expressing mice, resulting in the deletion of the *lox*P-flanked region. **c** Representative Southern blot showing the expected wild-type (WT) and recombined (Rec) hybridization signals at 9302 and 5794 bp, respectively, in embryonic stem cells from non-transfected (right column) and successfully transfected clones (left column). **d** Representative Western blot showing EGFP expression in spleen tissue homogenates from $CB_2^{EGFP/f/f}$ (left lane) and $CB_2^{-/-}$ mice (right lane). **e** The basal expression level of CB_2 receptor mRNA is not modified as a consequence of the insertion of the genetic construct used for the generation of the knock-in mice ($CB_2^{EGFP/f/f}$), as revealed by qRT-PCR in spleen samples and comparison with WT mice

containing exon 2 and downstream intronic sequences, (ii) a 2980 bp-sized fragment containing the coding part of exon 3 and upstream intronic sequences, and (iii) a 3657 bp-sized fragment containing the non-coding part of exon 3 and downstream sequences. The linearized targeting construct was transfected into C57BL/6J embryonic stem cells. Homologous recombinant cells were identified by Southern analysis and five clones were used to generate chimeric mice. Chimeras were bred with C57BL/6J Flp- and Cre-deleter females, in order to generate Neo-excised EGFP reporter knock-in ($CB_2^{EGFP/f/f}$) mice (Fig. 1a) and constitutive knock-out ($CB_2^{-/-}$) mice (Fig. 1b), respectively.

Homozygous mice identified by PCR were further verified by Southern blot analysis (Fig. 1c). All mice used in this study were fourth- or fifth-generation offspring from intercrosses of C57BL/6J mice. Mice were housed and bred in the animal facilities of Universidad Rey Juan Carlos (Alcorcón, Madrid, Spain) or the Medical College of Wisconsin (Milwaukee, WI, USA). Experimental protocols met the European and Spanish regulations for protection of experimental animals (86/609/EEC and RD 1201/2005 and 53/2013) or were approved by the Institutional Animal Care and Use Committee of the Medical College of Wisconsin. Male mice were used in all experiments included in the present report with the exception of flow cytometry experiments (see below).

Generation of $CB_2^{EGFP/f/f}$/5xFAD and $CB_2^{-/-}$/5xFAD mice

Mice co-expressing five familial Alzheimer's disease mutations (5xFAD) were purchased from Jackson Laboratories (Bar Harbor, ME, USA; [25]) on the C57BL/6J background and were mated with $CB_2^{EGFP/f/f}$ and $CB_2^{-/-}$ mice and backcrossed for at least five generations to generate $CB_2^{EGFP/f/f}$/5xFAD and $CB_2^{-/-}$/5xFAD mice. Animals employed in the present experiments were 3 to 6 months old; this period was chosen based on previously published data [25, 36] in order to allow for the appearance of amyloid deposits.

Flow cytometry

Single cell suspensions were prepared from the spleens of wild type, $CB_2^{EGFP/f/f}$, and $CB_2^{EGFP/f/+}$ mice of both sexes as described previously [27]. Cells were incubated with combinations of anti-mouse fluorescently-conjugated antibodies as follows: anti-B220 PE, anti-CD4 APC-eFluor780, anti-CD8 eFluor450, anti-CD11b eFluor450, anti-CD11c PE, anti-Ly6C APC, anti-Ly6G APC/Cy7, and anti-NK1.1 APC. Flow cytometry was used to identify B cells ($B220^+CD4^-CD8^-$), CD4 T cells ($CD4^+NK1.1^-$), CD8 T cells ($CD8^+$ $NK1.1^-$), NKT cells ($CD4^+NK1.1^+$), NK cells ($CD4^-NK1.1^+$), macrophages ($CD11b^+Ly6C^{+/-}Ly6G^-$), dendritic cells ($CD11b^+CD11c^{hi}$), and granulocytes ($CD11b^+Ly6C^+Ly6G^+$). Sample acquisition was performed on a BD Biosciences LSR II, and data was analyzed using FlowJo software to generate the geometric mean of eGFP expression in each immune cell population.

Immunofluorescence and neuritic plaque staining

Mice ($N = 4–6$ mice per group) were deeply anesthetized and transcardially perfused with cold PBS (pH 7.4) followed by freshly prepared cold 4% paraformaldehyde in PBS (pH 7.4). Tissue samples were collected and post-fixed in the same fixative overnight. Afterwards, tissues were dehydrated by sequential transfer to 10 and 30% sucrose solutions. Finally, tissues were cryoprotected with Tissue-Tek and frozen in dry ice. Thirty-micrometer-thick sections were obtained in a cryostat and preserved in cryoprotectant solution until use.

Floating tissue sections were washed with Tris Buffer Saline (TBS) before overnight incubation at 4 °C with the primary antibodies used for identification of the cellular types. For EGFP identification, overnight incubation with an anti-GFP antibody (1:1500; Abcam) was followed by incubation with an Alexa 488 anti-chicken antibody conjugate (Invitrogen) carried out at 37 °C for 2 h, rendering green fluorescence. Afterwards, sections were incubated with a rabbit polyclonal anti-ionized calcium-binding adaptor molecule 1 (Iba1) (1:1000 dilution, Wako, Osaka, Japan), diluted in TBS containing 1% bovine serum albumin (BSA; Sigma, St. Louis, USA) and 1% Triton x-100 (Sigma). After the incubation, sections were washed in TBS followed by incubation with an Alexa 546 anti-rabbit antibody conjugate (Invitrogen, Eugene, OR, USA) at 37 °C for 2 h, rendering red fluorescence. Additional tissue sections were incubated with mouse monoclonal anti-GFAP-Cy3 antibody (1:1500 dilution, Sigma) in the same buffer for 2 h at 37 °C or with mouse monoclonal anti-neuron-specific nuclear protein (NeuN) antibody (1:1000 dilution, Merck Millipore, Darmstadt, Germany) followed by incubation with Alexa 594 anti-mouse antibody conjugate (Invitrogen) as described above.

In order to study amyloid plaque deposits, a subset of $CB_2^{EGFP/f/f}$/5xFAD mice received an i.p. dose of 10 mg/kg of methoxy-XO4 (a Congo Red derivative known to selectively stain amyloid plaques; Tocris Bioscience; [4]) 24 h prior to sacrifice. Brains were processed and sections were obtained and preserved for immunostaining as described above.

Sections were mounted in aqueous solution (Vectashield, Vector Laboratories, Burlingame, CA, USA), coverslipped, and sealed. Slides were studied and photographed with upright microscopes (Nikon 90i, Nikon, Tokyo, Japan; and Axioimager M2, Zeiss, Oberkochen, Germany) and using a DXM1200F camera and C1 and LSM710 confocal systems [36]. Image analysis was carried out as described [36] with Metamorph (Molecular Devices, Sunnyvale, CA, USA) and ImageJ software (Research Services Branch, National Institute of Mental Health, Bethesda, MD, USA).

Western blotting

Protein fractions were collected from a Tri-pure extraction of hippocampal and spleen tissues, according to the manufacturer's instructions (Roche). Lysates (20 μg/lane or 10 μg/lane for hippocampal and spleen protein samples respectively) were separated by SDS-PAGE and transferred onto PVDF membranes (BioRad). After blocking in Tris-Tween buffered saline (TTBS; 10 mM Tris pH 7.5, 150 mM NaCl, 0.1% Tween 20 plus 5% nonfat dried milk), they were incubated overnight at 4 °C, as appropriate, with anti-GFP (1:500, Abcam, Cambridge, UK). Membranes were incubated with corresponding horseradish peroxidase-conjugated secondary antibody (1:8000) and were developed using a chemiluminescent reagent (ECL detection reagent GE Healthcare, Buckinghamshire, UK). Developed signals were recorded on X-ray film (Agfa) for densitometric analysis (ImageJ, NIH, MD, USA). $N = 4–6$ mice per group were used for protein quantification by Western blot.

ELISA $A\beta_{1\text{-}42}$

Human ELISA kits (Invitrogen, Camarillo, CA, USA) were used for the quantification of $A\beta_{1\text{-}42}$ in the brain soluble fractions, following the instructions provided by the manufacturer. Levels were normalized to the total amount of protein.

Real-time quantitative PCR for CB_2 and IL1β

Total RNA was isolated using Tripure Isolation Reagent (Roche, Mannheim, Germany) according to the protocol of the supplier. RNA was dissolved in RNase-free water and quantified by absorption at 260 nm. Aliquots were subjected to 1% denaturing agarose gel electrophoresis and GelRed Nucleic Acid Gel Stain (Biotium, Fremont, CA, USA) staining to verify the quantity and quality of RNA. Single-stranded complementary DNA (cDNA) was synthesized from 1 mg of total RNA using LightCycler Taqman Master (Roche Diagnostics). PCR primers and TaqMan probes were designed by Tib Molbiol (Berlin, Germany) (see Additional file 2: Figure S1). For normalization, 18S primers and probe number 55 from Universal ProbeLibrary (Roche) were utilized. Gene expression was quantified using LightCycler FastStart DNA Master HybProbe and LightCycler Taqman Master (Roche) and Quantimix Easy Probes kit (Biotools, Madrid, Spain) in a LightCycler thermocycler (Roche). The concentration of primers and probes were 0.5 and 0.2 μM, respectively. PCR assays were performed using 2 μl of the cDNA reaction. All assays were carried out twice as independent PCR runs for each cDNA sample. Mean values were used for further calculation. A negative (no template) control was measured in each of the PCR runs. Standard curves were calculated for quantification purposes using fivefold serial dilutions of cDNA from mouse brain. The transcript amounts were calculated using the second derivate maximum mode of the LC-software version 4.0. The specific transcript quantities were normalized to the transcript amounts of the reference gene 18S. All further calculations and statistical analyses were carried out with these values referred to as relative expression ratios.

Statistics

Results are expressed as mean ± SEM. Statistical analysis were made using student's t test for comparisons between two groups, analysis of variance (ANOVA), and two-way ANOVA with Tukey's post-test for multiple comparisons. A p value < 0.05 was considered as statistically significant (see Additional file 3: Table S1). Data were analyzed with Graph Pad Prism software version 6.0 (San Diego, CA, USA).

Results

Basal expression of EGFP in $CB_2^{EGFP/f/f}$ mouse spleen is coincident with previously described CB_2 receptor patterns of expression in immune cells

To characterize the newly generated $CB_2^{EGFP/f/f}$ mice, we performed Western blotting on spleen samples. A single band corresponding to the EGFP molecular weight was evident in $CB_2^{EGFP/f/f}$ mice and was undetectable in spleen samples from $CB_2^{-/-}$ mice (Fig. 1d). We determined whether the strategy for the generation of the knock-in mice modified the expression levels of CB_2R gene. Our results show that no changes were evident in CB_2R mRNA expression levels between WT and $CB_2^{EGFP/f/f}$ mice in spleen (Fig. 1e; $p = 0.474$), thus ruling out a putative impact of the transgene on basal expression of the receptor.

We used flow cytometry to identify and quantify the EGFP expression of splenocyte cell populations from wild type, $CB_2^{EGFP/f/+}$, and $CB_2^{EGFP/f/f}$ mice (Fig. 2a–c). Using wild type mice, we found that background EGFP immunofluorescence was low in all immune cell populations examined (Fig. 2a). EGFP expression levels in splenic immune cells were compared in heterozygous (Fig. 2b) and homozygous (Fig. 2c) $CB_2^{EGFP/f/f}$ mice. In all immune cell populations investigated, the homozygous $CB_2^{EGFP/f/f}$ mice exhibited approximately double the mean fluorescence intensity (MFI) of the heterozygous mice. EGFP expression was highest in the B cell population, which is consistent with reports that B cells have the highest CB_2 receptor expression among these cell types [12]. Among the T cell populations, CD4 T cells and NK T cells expressed a similar low level of EGFP expression, while CD8 T cells expressed ~threefold higher levels (Fig. 2). NK cells expressed negligible levels of EGFP (Fig. 2). Monocytes/macrophages and dendritic cells expressed EGFP in a broader expression

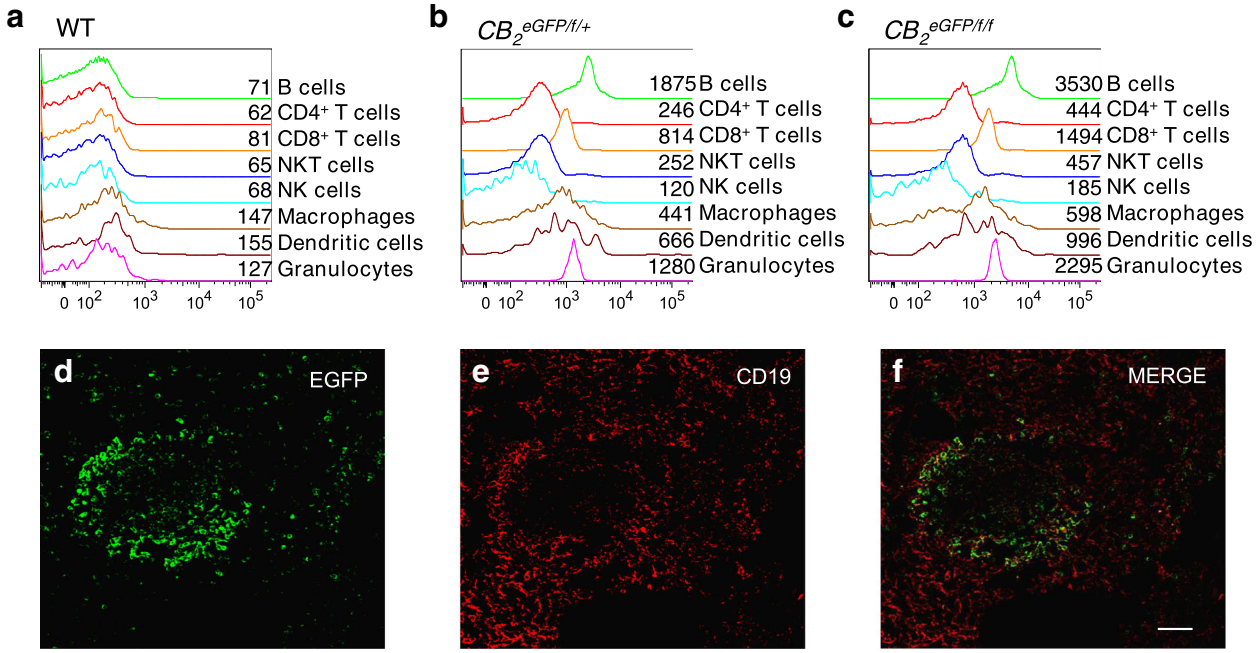

Fig. 2 EGFP presence and distribution in $CB_2^{EGFP/f/}$ spleens determined using flow cytometry (**a**–**c**) and immunofluorescence (**d**–**f**). **a**–**c** Determination of cell-specific expression of EGFP in splenocytes harvested from WT (**a**), $CB_2^{EGFP/f/+}$ (**b**), and $CB_2^{EGFP/f/f}$ (**c**) mice. The numbers next to the histograms are the mean fluorescence intensity (MFI). **d**–**f** CB_2-dependent-EGFP expression in B-lymphocytes in the spleen of $CB_2^{EGFP/f/f}$. EGFP expression was evident in follicles of the white pulp. Scale bars, 100μm (**d**–**g**)

pattern than the lymphocytes (Fig. 2). Given that the spleen contains numerous macrophage and dendritic cell populations, it is likely that CB_2R, and thus EGFP, will be differentially expressed among them [7, 15]. Finally, of the myeloid subset, granulocytes exhibited the highest amount of EGFP expression. These data are consistent with the published reports of CB_2R distribution among these cell types [12] indicating that the $CB_2^{EGFP/f/f}$ mouse is an excellent tool by which to determine steady state CB_2R expression in various spleen cell populations using EGFP fluorescence.

We analyzed the expression of EGFP in spleens of $CB_2^{EGFP/f/f}$ mice by immunofluorescence and found discrete cell populations showing detectable signal. $EGFP^+$ B cells were detected, limited to the marginal zone of the white pulp follicles, mostly located in the follicular corona (Fig. 2d–f).

Basal expression of EGFP in $CB_2^{EGFP/f/f}$ mice is undetectable in the CNS but is induced as a consequence of amyloid deposition

In the CNS, microscopic analysis of the brain and spinal cord of 3-, 4-, or 6-month-old $CB_2^{EGFP/f/f}$ mice showed no detectable EGFP immunoreactivity above background in glial or neuronal elements of any region examined, which included hippocampus (Fig. 3a), cortex, cerebellum, thalamus, brain stem, and spinal cord (not shown). In contrast, intense EGFP signal could be seen in brain regions of $CB_2^{EGFP/f/f}$/5xFAD mice known to be rich in beta-amyloid neuritic plaques, such as hippocampus (Fig. 3b). Other regions such as cortex, thalamus, and brain stem also exhibited EGFP signal (data not shown), in concordance with the previously reported distribution of neuritic plaques [25]. $EGFP^+$ cells exhibited an ameboid shape and were mostly found in clusters (Fig. 3c), suggesting they could be activated microglial cells. No signal could be observed in the hippocampus of $CB_2^{-/-}$/5xFAD mice (Fig. 3d) or in any other brain region examined (data not shown).

As shown in Fig. 3e, EGFP immunoreactivity above background could be observed as early as 3 months of age in the $CB_2^{EGFP/f/f}$/5xFAD mice, and EGFP-labeled cells increased in density with age in these mice (Fig. 3e–h). $EGFP^+$ were found in clusters throughout the brain parenchyma and their distribution and increased density with age paralleled that of neuritic plaques, identified using methoxy-XO4, a dye for amyloid deposits (Fig. 3i–l). Interestingly, no EGFP signal could be observed in regions not exhibiting neuritic plaques (asterisks in Fig. 3g–k). The number of $EGFP^+$ cells was dramatically increased at 4 and 6 months of age, which also paralleled the increase in the appearance of amyloid deposits (Fig. 3h: $F_{3,18} = 58.46$, $p < 0.0001$; Fig. 3l: $F_{3,23} = 64.70$, $p < 0.0001$).

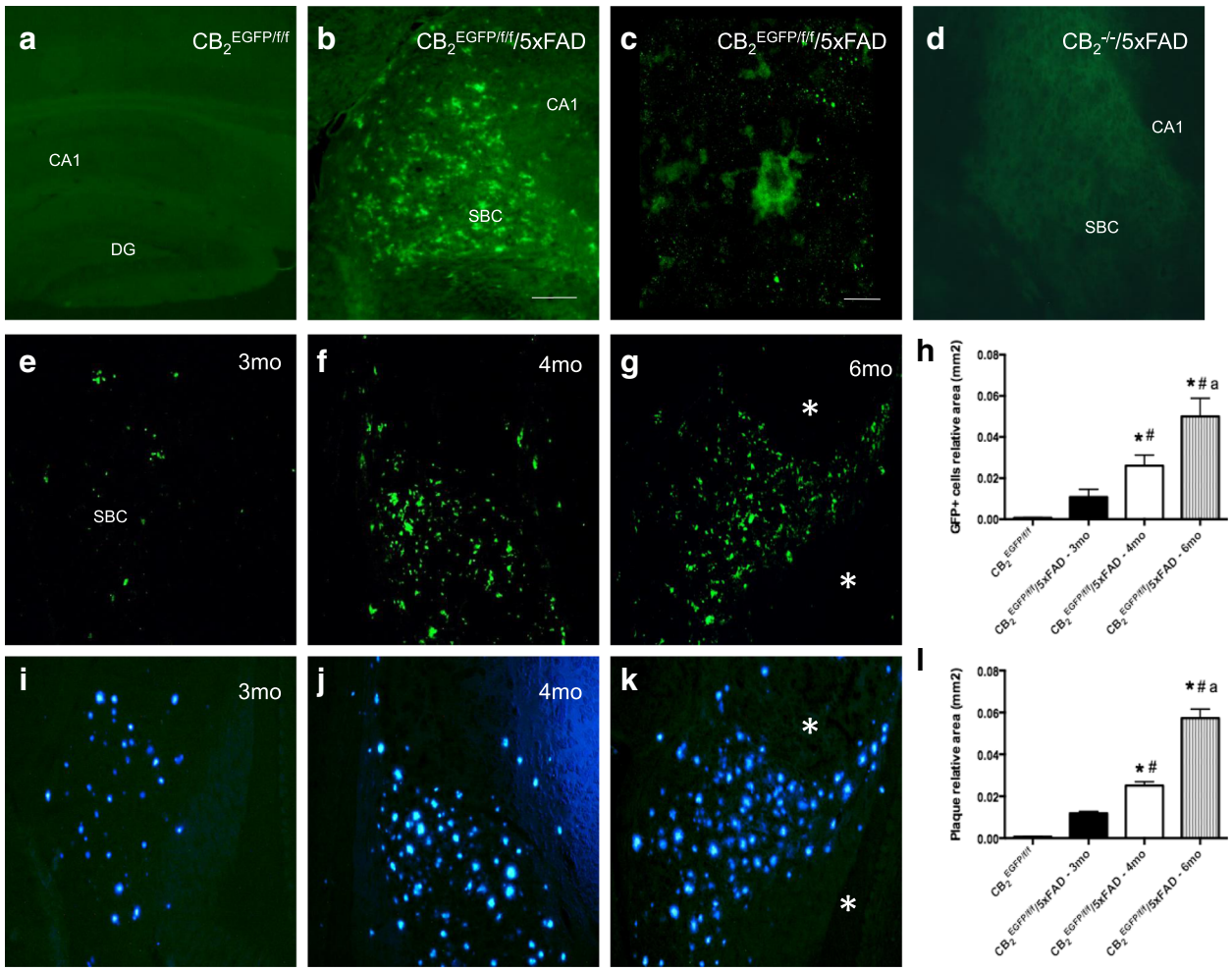

Fig. 3 In vivo EGFP induction in the context of AD, as revealed by immunofluorescence. **a** Un-manipulated, healthy $CB_2^{EGFP/f/f}$ mice showed no significant EGFP signal in hippocampus (**a**). **b**, **c** EGFP signal could be noticed in the brain of $CB_2^{EGFP/f/f}$/5xFAD mice; these cells showed ameboid shape. **d** No EGFP signal could be observed in any brain region of $CB_2^{-/-}$/5xFAD mice, including those enriched in amyloid plaques such as hippocampus. **e**–**l** EGFP signal in $CB_2^{EGFP/f/f}$/5xFAD mice increased with age and paralleled that of amyloid deposits. EGFP was evident in brain samples of $CB_2^{EGFP/f/f}$/5xFAD mice starting at 3 months of age (**e**) and progressively increasing with age (4 months, **f**, and 6 months, **g**) and matched with the pattern of distribution of amyloid-enriched plaques stained with methoxy-XO4 in those same samples (figure **i**–**k**). Note that neighboring brain regions devoid of amyloid deposits exhibited a complete absence of EGFP signal (asterisks in **g**, **k**). **h**, **l** Densitometric quantification of $EGFP^+$ cells (**h**) and amyloid plaques (**k**) shows a parallel increase in neuritic plaques and EGFP expression. Data are expressed as mean ± SEM. *$p < 0.05$ vs $CB_2^{EGFP/f/f}$ mice, # vs $CB_2^{EGFP/f/f}$/5xFAD-3mo mice, and "a" vs $CB_2^{EGFP/f/f}$/5xFAD-4mo mice. $N = 5$ for immunofluorescence labeling. Scale bars, 10 μm (**c**) and 50 μm. DG (dentate gyrus); SBC (subiculum); CA1 (CA1 region of Ammon's horn)

CB_2R induction is limited to plaque-associated microglial cells

$EGFP^+$ cells were located in association with neuritic plaques (as revealed by staining with methoxy-XO4) and exhibited morphological features of microglia (Fig. 4). Co-localization studies with Iba-1, a commonly used marker of cells of myeloid lineage, were carried out. Low magnification (a to d) images showed a match in the pattern of distribution among $EGFP^+$ and $Iba1^+$ cells in the subiculum of 6-month-old $CB_2^{EGFP/f/f}$/5xFAD mice; in addition, our data show that CB_2-dependent EGFP expression takes place selectively in $Iba1^+$ cells located in the vicinity of neuritic plaques (Fig. 4e–l). Microglial cells not associated with these pathological structures showed no EGFP staining (see Fig. 5a–d). For example, note the microglial cell at the arrow in Fig. 5b is neither EGFP positive nor associated with a plaque. Differences in the morphological features of $EGFP^+$ and $EGFP^-$ microglial cells were evident, with $EGFP^+$ cells exhibiting an ameboid-like shape (Fig. 5a and b), typical of activated microglia, while $EGFP^-$ cells showed a highly ramified morphology, characteristic of quiescent, non-activated, microglia (arrow in Fig. 5b).

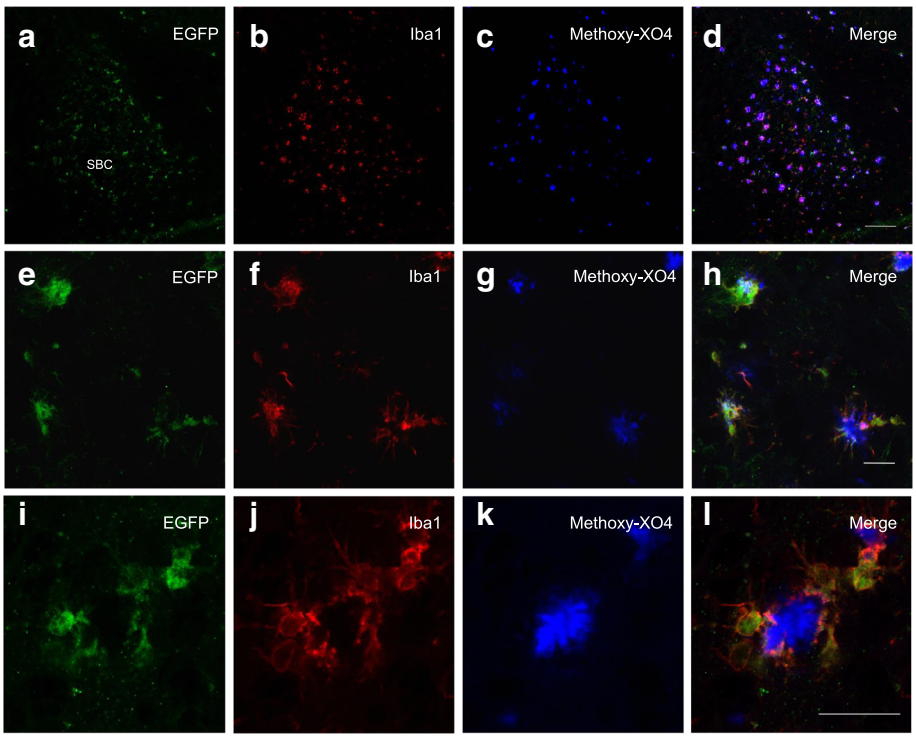

Fig. 4 Restricted EGFP expression in microglial cells located in peri-plaque areas of the $CB_2^{EGFP/f/f}$/5xFAD mouse hippocampus. **a**–**l** Low-magnification photographs of $EGFP^+$ microglial cells (**a**, **b**) in close association to beta-amyloid neuritic plaques (**c**, **d**). Medium- (**e**–**h**) and high-magnification (**i**–**l**) photographs of $EGFP^+$ microglial cells. Detailed co-localization immunofluorescent analysis reveals a complete overlap between $EGFP^+$ cells and $Iba1^+$ cells, indicative of their macrophage/microglia nature, and a selective association to amyloid-enriched plaques (stained with methoxy-XO4). Scale bars, 100 μm (**a**–**d**), 25 μm (**e**–**h**), and 25 μm (**i**–**l**). SBC (subiculum)

Furthermore, we also studied whether other cell types in the CNS, such as neurons or astrocytes expressed EGFP in $CB_2^{EGFP/f/f}$/5xFAD mice. To that end, co-localization studies with a neuronal marker (NeuN; Fig. 5e–h) or with a marker of astrocytes (GFAP; Fig. 5i–l) were carried out. Our data indicate that neither of these cell types express EGFP; thus, *cnr2*-dependent EGFP expression is limited to microglial cells in $CB_2^{EGFP/f/f}$/5xFAD mice.

Changes associated with CB_2R deletion include decreases in plaque deposition and no changes in gliosis or IL1β expression

We analyzed the impact of *cnr2* gene deletion on plaque formation, soluble amyloid levels and neuroinflammation (Fig. 6). We found a small but significant decrease in hippocampal neuritic plaque density (measured by staining with methoxy-XO4; Fig. 6a: $p < 0.0338$) in the $CB_2^{-/-}$ mice that was not paralleled by changes in soluble levels of $A\beta_{1\text{-}42}$ in the hippocampus (measured by ELISA; Fig. 6b: $p < 0.6413$). Hippocampal microgliosis was assessed by counting $Iba1^+$ cells in tissue sections. As expected, the 5xFAD mice exhibited a significant increase in $Iba1^+$ cells (Fig. 6c: $F_{1,23} = 85.84$, $p < 0.0001$); however, there was no difference in this measure between the wild type and $CB_2^{-/-}$ mice (Fig. 6c: $F_{1,23} = 0.03775$, $p = 0.8476$). Finally, a significant increase in interleukin-1 beta (IL1β) was observed as a consequence of the amyloid pathology (Fig. 6d: $F_{1,23} = 49.12$, $p < 0.0001$) but CB_2R genotype had no effect ($F_{1,33} = 0.2229$, $p = 0.6400$).

Discussion

We have established a novel transgenic mouse model ($CB_2^{EGFP/f/f}$) that allows for identification of cells that are actively transcribing the *cnr2* gene. The use of an IRES allows for coupling of EGFP expression to *cnr2* gene transcription without loss or modification of the CB_2 protein, which is a different approach from another reporter mouse line in which the *cnr2* gene is replaced by EGFP, resulting in a CB_2R knock out [29, 30]. The present reporter mice are expected to provide crucial information on the distribution, expression, and pathophysiological roles of the CB_2R, while maintaining its appropriate cellular expression. By crossing these mice with 5xFAD mice, we have expanded our knowledge regarding the relevance of CB_2R in amyloid pathology. The main conclusions of this study are that, if CB_2R are expressed by neurons or glia in the CNS of healthy, un-manipulated mice, they are expressed at very low turnover rates

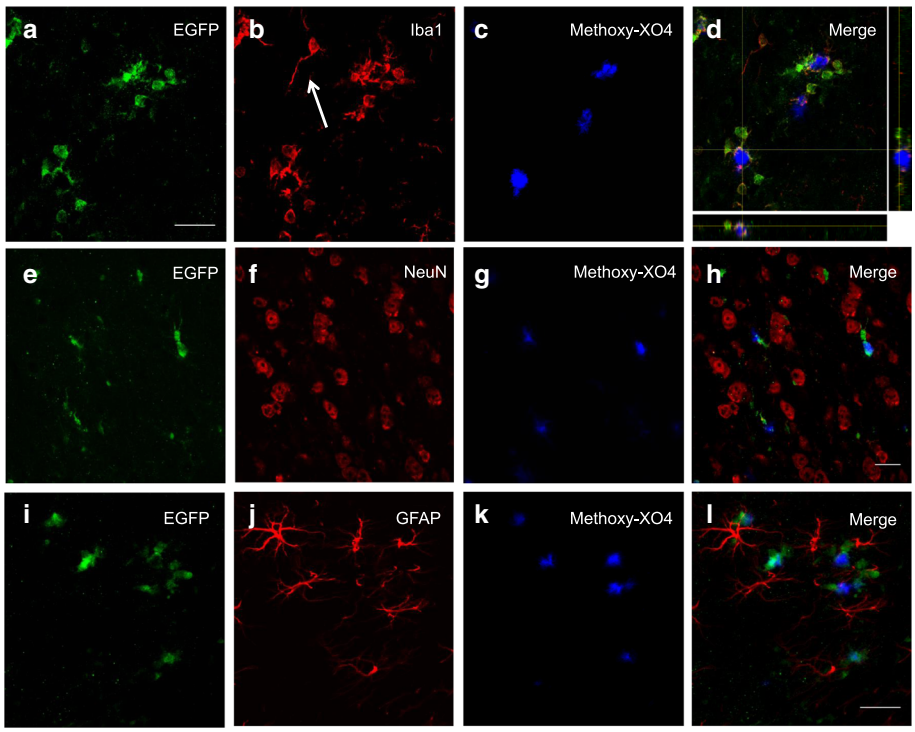

Fig. 5 EGFP expression is limited to plaque-associated microglial cells but is absent in neurons and astrocytes in $CB_2^{EGFP/f/f}$/5xFAD mice. **a**–**c** Z-stack showing that EGFP expression (**a**) was evident in microglial cells (**b**) located in close association to amyloid-enriched neuritic plaques, as revealed by methoxy-XO4 (**c**). However, microglial cells not linked with these pathological structures (arrow in **b**) showed reduced EGFP signal. **d** Orthogonal view in *Z* axis of the cluster of microglial $EGFP^+$ cells shown in (**a**–**c**). Note the intimate contact established by microglial processes into the neuritic plaque. **e**–**l** Neurons ($NeuN^+$ cells; **e**–**h**) nor astrocytes ($GFAP^+$ cells; **i**–**l**) showed no EGFP signal. Scale bars, 25 μm

because no specific EGFP signaling could be detected in any region of the mouse brain or spinal cord. Second, under chronic neuroinflammatory stimuli (such as those derived from the deposition of the amyloid peptide in the brain parenchyma), the expression of CB_2R is induced in microglial cells, and this induction takes place specifically in activated microglial cells surrounding neuritic plaques. These data confirm and expand previously published literature and support the contention that the presence of CB_2R may be a diagnostic marker of neuroinflammation in the context of AD [5, 6] and other pathological conditions with a neuroinflammatory component [19, 20].

As previously suggested by us and by others [5, 19, 26], the expression of CB_2R is induced under neuroinflammatory conditions in the human brain, being restricted to microglial cells closely associated to foci of neuroinflammation. Data obtained from samples of humans affected by several neurodegenerative conditions with accompanying neuroinflammation (i.e., AD, MS, HIV-encephalitis) revealed a consistent pattern of CB_2R induction in microglia [6]. Our present data expand and confirm these observations. We used a well-known mouse model of amyloid pathology (5xFAD) to calibrate the impact that the appearance of neuritic plaques in the brain parenchyma has on the expression of CB_2R. The analysis of $CB_2^{EGFP/f/f}$/5xFAD mice brain tissues showed that *cnr2*-dependent EGFP expression is present in microglial ($Iba1^+$) cells located in the vicinity of amyloid-enriched neuritic plaques (as revealed with methoxy-XO4 in vivo staining). There was a remarkable lack of detectable EGFP expression in non-plaque areas. These data strongly support the hypothesis that CB_2R gene expression is increased primarily in microglia that surround neuritic plaques.

The time-course of the appearance of neuritic plaques in the subiculum of $CB_2^{EGFP/f/f}$/5xFAD mice closely matched that previously described [25, 36]. Importantly, EGFP was detectable in plaque-associated microglia at 3 months of age, corresponding to the age when amyloid deposits are first present in the brain parenchyma. These data are indicative of the need to reach a threshold of inflammatory stimuli in the cellular milieu before the induction of CB_2R expression takes place in the CNS. The present data suggest that threshold is reached coincident with appearance of the amyloid deposits. This suggests (i) that the induction of the expression of CB_2 receptors takes place after a period of sustained inflammation and (ii) that CB_2 receptors may be postulated as early markers of AD pathology. In this sense, it is important to note that disease-linked symptoms in 5xFAD mice are not evident before 6 months of age; thus, the

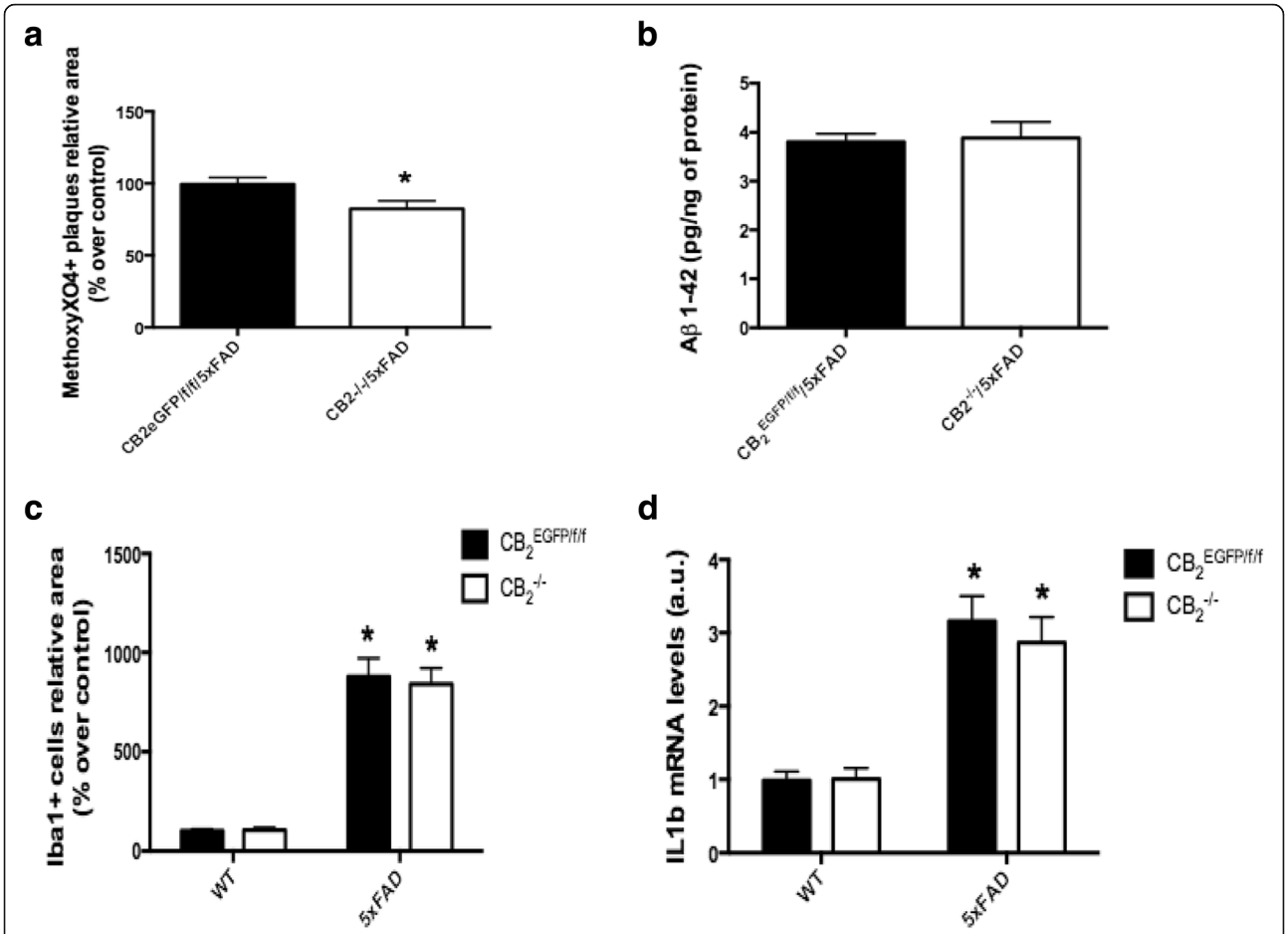

Fig. 6 Consequences of CB_2 deletion in the context of AD. The genetic inactivation of CB_2 in $CB_2^{-/-}$/5xFAD mice led to a significant decrease in plaque density in hippocampus (**a**), without any changes in soluble amyloid production (**b**), or microgliosis (**c**). No changes were observed in the expression of IL1β as a consequence of gene deletion (**d**) in $CB_2^{-/-}$/5xFAD mice as compared to those in $CB_2^{EGFP/f/f}$/5xFAD mice. Data are expressed as mean ± SEM. *$p < 0.05$. Student's *t*-test (**a**, **b**) and two-way ANOVA followed by Tukey's post hoc test (**c**, **d**). $N = 5$ for immunofluorescence labeling measurements and $N = 6$ for experiments on soluble amyloid quantification and IL1β expression

induction of the *cnr2* gene expression is previous to phenotypic changes due to amyloid pathology, indicating that CB_2R may provide diagnostic and therapeutic targets for the treatment of early stage AD [28].

CB_2R functions in microglia as well as in other types of immune cells have been studied [8, 20]. In the context of AD neuroinflammation, there is evidence that CB_2R agonists induce anti-inflammatory actions [1, 10, 21, 22, 26, 34], promote microglial migration and proliferation [37], and enhance amyloid removal [33, 38]. Furthermore, there is evidence that the activation of CB_2R also decreases the production of amyloid peptides in a mouse model of AD [2], though conflicting results have been reported [29]. These effects make microglial CB_2R interesting targets in amyloid-induced neuroinflammation as microglia play critical roles in the progression of the disease by modulating, for instance, amyloid removal, cytokine production or exosome-mediated peptide degradation [14].

Surprisingly in light of earlier studies, $CB_2^{-/-}$/5xFAD mice exhibited a small but significant decrease in neuritic plaque density in hippocampus compared to wild type 5xFAD mice that was not accompanied by a decrease in soluble $A\beta_{1\text{-}42}$ levels, reduced microgliosis, or changes in IL1β expression. We do not have a conclusive explanation for this observation, though it is suggestive of a role for CB_2R in microglial functions related to amyloid removal such as, for instance, phagocytosis [33]. In addition, conflicting results have been reported by several groups regarding the consequences of CB_2 deletion on microgliosis, with both decreased and unchanged microgliosis being reported [2, 16, 30]. Further experiments are needed to clarify the reasons for these discrepancies regarding the impact of CB_2R deletion on the formation of amyloid-enriched plaques.

Several recent studies indicate that CB_2R agonists affect neuronal function [11, 32, 39]. In particular, CB_2R

agonists have been reported to affect hippocampal plasticity, effects that are lost in $CB_2^{-/-}$ mice. These results are difficult to reconcile in light of the lack of detectable EGFP in the hippocampus of the present transgenic mice and in another reporter model [29]. It is possible that the turnover of the CB_2R in neurons is slower than the turnover of EGFP protein or the detectable amount of EGFP expression may be lower than the CB_2R expression levels required to achieve a functional response in vivo. Alternatively, it is possible that CB_2R expression is upregulated by the processes involved in the preparation of tissues for study ex vivo.

Our data are discordant compared to those reported in the Allen Mouse Brain Atlas [17]. Information provided by this platform reveals low but detectable levels of CB_2-mRNA in olfactory and cortical subplate areas, as shown by single cell in situ hybridization (ISH). However, neither $CB_2^{EGFP/f/f}$ nor $CB_2^{EGFP/f/f}$/5xFAD mice showed specific EGFP signal in either of these regions. We do not have an explanation for this discrepancy other than the mentioned mismatch between detection limits, in this case referred to single cell-ISH (Allen Atlas) and EGFP immunostaining (present data).

Conclusions

In summary, the present findings confirm and expand previous data showing the selective induction of CB_2R in neuritic plaque-associated microglia and postulate these receptors as diagnostic and therapeutic targets in AD. The newly developed transgenic mouse model will be instrumental for elucidating their role(s) in neuroinflammatory conditions.

Additional files

Additional file 1: CB2 Western blots. Test of different CB2 primary antibodies in spleen samples (with high CB2 expression levels in normal conditions) harvested from CB2EGFP mice (lines 1, 2, and 3) and CB2KO mice (lines 4, 5, and 6). GFP and beta-actin immunodetection was employed as internal controls. (PPTX 6471 kb)

Additional file 2: Figure S1. Sequences of the primers employed in the present studies. (DOCX 13 kb)

Additional file 3: Table S1. Statistical analysis of the data provided in the manuscript. (DOCX 17 kb)

Abbreviations

5xFAD: Mice co-expressing five familial Alzheimer's disease mutations; AD: Alzheimer's disease; BSA: Bovine serum albumin; CB_2R: Cannabinoid receptor, subtype 2; CD4: Cluster of differentiation 4; CNS: Central nervous system; EGFP: Enhanced green fluorescent protein; ELISA: Enzyme-linked immunosorbent assay; GFAP: Glial fibrillary acidic protein; i.p.: Intraperitoneal; Iba1: Ionized calcium-binding adaptor molecule 1; IL1β: Interleukin-1 beta; IRES: Internal Ribosomal Entry Site; ISH: In situ hybridization; NeuN: Neuron-specific nuclear protein; PBS: Phosphate buffered saline; PVDF: Polyvinylidene fluoride; qRT-PCR: Quantitative real-time polymerase chain reaction; SDS-PAGE: Sodium dodecyl sulfate polyacrylamide gel electrophoresis; THC: Δ^9-tetrahydrocannabinol; TTBS: Tris-Tween buffer saline; UTR: Untranslated region

Acknowledgements

A.L.V. (BES-2014-070233) and C.V. (BES-2011-043393) are recipients of FPI predoctoral fellowships from the Ministerio de Economía y Competitividad. N.A. and G.R-P. are recipients of predoctoral fellowships from Universidad Francisco de Vitoria. I.B-C. is a recipient of a postdoctoral fellowship from Comunidad Autónoma de Madrid (PEJD-2017-POST/BMD-4478).

Funding

This work was supported by the Ministerio de Economía y Competitividad (SAF2013/42797-R and SAF2016/75959-R, JR), Ministerio de Educación of Spain (PR2009-0169, JR), Comunidad de Madrid (S2010/BMD-2308, JR), Universidad Francisco de Vitoria (2017, JR), and the Research Component of the Advancing a Healthier Wisconsin Endowment at the Medical College of Wisconsin (CJH), the National Institute on Drug Abuse (DA041212, CJH), and the National Multiple Sclerosis Society (RG 4432-A-5, BND).

Availability of data and materials

The datasets used and/or analyzed during the current study are available from the corresponding author on a reasonable request.

Authors' contributions

CJH and JR conceived and designed the experiments. AL, NA, MRP, MTG, MABM, IBC, CV, MA, GRP, EGG, MB, RMT, BND, and JR performed the experiments. RMT, BND, CJH, and JR analyzed the data. BND, CJH, and JR wrote the manuscript. All authors read and approved the manuscript.

Ethics approval

Experimental protocols met the European and Spanish regulations for protection of experimental animals (86/609/EEC and RD 1201/2005 and 53/2013) or were approved by the Institutional Animal Care and Use Committee of the Medical College of Wisconsin.

Competing interests

The authors declare that they have no competing interests.

Publisher's Note

Author details

[1]Laboratorio de Apoyo a la Investigación, Hospital Universitario Fundación Alcorcón, C/ Budapest 1, 28922 Alcorcón, Madrid, Spain. [2]Universidad Rey Juan Carlos, Móstoles, Spain. [3]Faculty of Experimental Sciences, Universidad Francisco de Vitoria, 28223 Pozuelo de Alarcón, Madrid, Spain. [4]Blood Research Institute, BloodCenter of Wisconsin, Milwaukee, WI 53226, USA. [5]Department of Pharmacology and Neuroscience Research Center, Medical College of Wisconsin, Milwaukee, WI 53226, USA.

Received: 11 January 2018 Accepted: 23 April 2018
Published online: 24 May 2018

References

1. Aso E, Juvés S, Maldonado R, Ferrer I. CB2 cannabinoid receptor agonist ameliorates Alzheimer-like phenotype in AβPP/PS1 mice. J Alz Dis. 2013; 35:847-858.
2. Aso E, Andrés-Benito P, Carmona M, Maldonado R, Ferrer I. Cannabinoid receptor 2 participates in amyloid-β processing in a mouse model of Alzheimer's disease but plays a minor role in the therapeutic properties of a cannabis-based medicine. J Alz Dis. 2016;51:489-500.
3. Atwood BK, Mackie K. CB2: a cannabinoid receptor with an identity crisis. Br J Pharmacol. 2010;160:467–79.
4. Bacskai BJ, Klunk WE, Mathis CA, Hyman BT. Imaging amyloid-β deposits in vivo. J Cereb Blood Flow Metab. 2002;22:1035-1041.
5. Benito C, Nunez E, Tolon RM, Carrier EJ, Rabano A, Hillard CJ, Romero J. Cannabinoid CB2 receptors and fatty acid amide hydrolase are selectively overexpressed in neuritic plaque-associated glia in Alzheimer's disease brains. J Neurosci. 2003;23:11136–41.
6. Benito C, Tolon RM, Pazos MR, Nuñez E, Castillo AI, Romero J. Cannabinoid CB2 receptors in human brain inflammation. Br J Pharmacol. 2008;153:277–85.

7. Borges da Silva H, Fonseca R, Pereira RM, Cassado Ados A, Álvarez JM, D'Império Lima MR. Splenic macrophage subsets and their function during blood-borne infections. Front Immunol. 2015;6:480.
8. Cabral GA, Ferrerira GA, Jamerson MJ. Endocannabinoids and the immune system in health and disease. Handb Exp Pharmacol. 2015;231:185–211.
9. Carlisle SJ, Marciano-Cabral F, Staab A, Ludwick C, Cabral GA. Differential expression of the CB2 cannabinoid receptor by rodent macrophages and macrophage-like cells in relation to cell activation. Int Immunopharmacol. 2002;2:69–82.
10. Esposito G, Iuvone T, Savani C, Scuderi C, De Filippis D, Papa M, DiMarzo V, Steardo L. Opposing control of cannabinoid receptor stimulation on amyloid-beta-induced reactive gliosis: in vitro and in vivo evidence. J Pharmacol Exp Ther. 2007;322:1144–52.
11. Foster DJ, Wilson JM, Remke DH, Mahmood MS, Uddin MJ, Wess J, Patel S, Marnett LJ, Niwswender CM, Jones CK, Xiang Z, Lindsley CW, Rook JM, Conn PJ. Antipsychotic-like effects of M4 positive allosteric modulators are mediated by CB2 receptor-dependent inhibition of dopamine release. Neuron. 2016;91:1244–52.
12. Galiègue S, Mary S, Marchand J, Dussossoy D, Carrière D, Carayon P, Bouaboula M, Shire D, Le Fur G, Casellas P. Expression of central and peripheral cannabinoid receptors in human immune tissues and leukocyte subpopulations. Eur J Biochem. 1995;232:54–61.
13. Gong JP, Onaivi ES, Ishiguro H, Liu QR, Tagliaferro PA, Brusco A, Uhl GR. Cannabinoid CB2 receptors: immunohistochemical localization in rat brain. Brain Res. 2006;1071:10–23.
14. Heneka MT, Golenbock DT, Latz E. Innate immunity in Alzheimer's disease. Nat Immunol. 2015;16:229–36.
15. Hey YY, O'Neill HC. Murine spleen contains a diversity of myeloid and dendritic cells distinct in antigen presenting function. J Cell Mol Med. 2012;16:2611–9.
16. Koppel J, Vingtdeux V, Marambaud P, D'Abramo C, Jimenez H, Stauber M, Friedman R, Davies P. CB2 receptor deficiency increases amyloid pathology and alters tau processing in a transgenic mouse model of Alzheimer's disease. Mol Med. 2014;20:29–36.
17. Lein ES, et al. Genome-wide atlas of gene expression in the adult mouse brain. Nature. 2007;445:168–76.
18. Lynn AB, Herkenham M. Localization of cannabinoid receptors and nonsaturable high-density cannabinoid binding sites in peripheral tissues of the rat: implications for receptor-mediated immune modulation by cannabinoids. J Pharmacol Exp Ther. 1994;268:1612–23.
19. Maresz K, Carrier EJ, Ponomarev ED, Hillard CJ, Dittel BN. Modulation of the cannabinoid CB2 receptor in microglial cells in response to inflammatory stimuli. J Neurochem. 2005;95:437–45.
20. Maresz K, Pryce G, Ponomarev ED, Marsicano G, Croxford JL, Shriver LP, Ledent C, Cheng X, Carrier EJ, Mann MK, Giovannoni G, Pertwee RG, Yamamura T, Buckley NE, Hillard CJ, Lutz B, Baker D, Dittel BN. Direct supression of CNS autoimmune inflammation via the cannabinoid receptor CB1 on neurons and CB2 on autoreactive T cells. Nat Med. 2007;13:492–7.
21. Martín-Moreno AM, Reigada D, Ramírez G, Mechoulam R, Innamorato N, Cuadrado A, de Ceballos ML. Cannabidiol and other cannabinoids reduce microglial activation in vitro and in vivo: relevance to Alzheimer's disease. Mol Pharmacol. 2011;79:964–73.
22. Martín-Moreno AM, Brera B, Spuch C, Carro E, García-García L, Delgado M, Pozo MA, Innamorato NG, Cuadrado A, de Ceballos ML. Prolonged oral cannabinoid administration prevents neuroinflammation, lowers beta-amyloid levels and improves cognitive performance in Tg APP2576 mice. J Neuroinflamm. 2012;9:8.
23. Munro S, Thomas KL, Abu-Shaar M. Molecular characterization of a peripheral receptor for cannabinoids. Nature. 1993;365:61–5.
24. Nuñez E, Benito C, Pazos MR, Barbachano A, Fajardo O, González S, Tolón RM, Romero J. Cannabinoid CB2 receptors are expressed by perivascular microglial cells in the human brain: an immunohistochemical study. Synapse. 2004;53:208–13.
25. Oakley H, Cole SL, Logan S, Maus E, Shao P, Craft J, Guillozet-Bongaarts A, Ohno M, Disterhoft J, Van Eldik L, Berry R, Vassar R. Intraneuronal beta-amyloid aggregates, neurodegeneration, and neuron loss in transgenic mice with five familial Alzheimer's disease mutations: potential factors in amyloid plaque formation. J Neurosci. 2006;26:10129–40.
26. Ramírez BG, Blázquez C, Gómez del Pulgar T, Guzmán M, de Ceballos ML. Prevention of Alzheimer's disease pathology by cannabinoids: neuroprotection mediated by blockade of microglial activation. J Neurosci. 2005;23:1904–13.
27. Ray A, Basu S, Gharalbeth RZ, Cook LC, Kumar R, Lefkowitz EJ, Walker CR, Morrow CD, Franklin CL, Gelger TL, Salzman NH, Fodor A, Dittel BN. Gut microbial dysbiosis due to helicobacter drives an increase in marginal zone B cells in the absence of IL-10 signaling in macrophages. J Immunol. 2015; 195:3071–85.
28. Savonenko AV, Melnikova T, Wang Y, Ravert H, Gao Y, Koppel J, Lee D, Pletnikova O, Cho E, Sayyida N, Hiatt A, Troncoso J, Davies P, Dannals RF, Pomper MG, Horti AG. Cannabinoid CB2 receptors in a mouse model of Ab amyloidosis: immunohistochemical analysis and suitability as a PET biomarker of neuroinflammation. PLoS One. 2015;10 https://doi.org/10.1371/journal.pone.0129618. eCollection 2015
29. Schmöle AC, Lundt R, Gennequin B, Schrage H, Beins E, Krämer A, Zimmer T, Limmer A, Zimmer A, Otte DM. Expression analysis of CB2-GFP BAC transgenic mice. PLoS One. 2015a;10 https://doi.org/10.1371/journal.pone.0138986. eCollection 2015
30. Schmöle AC, Lundt R, Ternes S, Albayram Ö, Ulas T, Schultze JL, Bano D, Nicotera P, Alferink J, Zimmer A. Cannabinoid receptor 2 deficiency results in reduced neuroinflammation in an Alzheimer's disease mouse model. Neurobiol Ag. 2015b;36:710–9.
31. Stella N. Cannabinoid and cannabinoid-like receptors in microglia, astrocytes, and astrocytomas. Glia. 2010;58:1017–30.
32. Stempel AV, Stumpf A, Zhang HY, Özdögan T, Pannasch U, Theis AK, Otte DM, Wojtalla A, Racz I, Ponomarenko A, Xi ZX, Zimmer A, Schimtz D. Cannabinoid type 2 receptors mediate a cell type-specific plasticity in the hippocampus. Neuron. 2016;90:795–809.
33. Tolón RM, Núñez E, Pazos MR, Benito C, Castillo AI, Martínez-Orgado JA, Romero J. The activation of cannabinoid CB2 receptors stimulates in situ and in vitro beta-amyloid removal by human macrophages. Brain Res. 2009; 1283:148–54.
34. Van der Stelt M, Mazzola C, Esposito G, Matias I, Petrosino S, De Filippis D, Micale V, Steardo L, Drago F, Iuvone T, Di Marzo V. Endocannabinoids and beta-amyloid-induced neurotoxicity in vivo: effect of pharmacological elevation of endocannabinoid levels. Cell Mol Life Sci. 2006;63:1410–24.
35. Van Sickle MD, Duncan M, Kingsley PJ, Mouihate A, Urbani P, Mackie K, Stella N, Makriyannis A, Piomelli D, Davison JS, Marnett LJ, Di Marzo V, Pittman QJ, Patel KD, Sharkey KA. Identification and functional characterization of brainstem cannabinoid CB2 receptors. Science. 2005;310:329–32.
36. Vazquez C, Tolón RM, Grande MT, Caraza M, Moreno M, Koester EC, Villaescusa B, Ruiz-Valdepeñas L, Fernández-Sánchez FJ, Cravatt BF, Hillard CJ, Romero J. Endocannabinoid regulation of amyloid-induced neuroinflammation. Neurobiol Ag. 2015;36:3008–19.
37. Walter L, Franklin A, Witting A, Wade C, Xie Y, Kunos G, Mackie K, Stella N. Nonpsychotropic cannabinoid receptors regulate microglial cell migration. J Neurosci. 2003;23:1398–405.
38. Wu J, Bie B, Yang H, Xu JJ, Brown DL, Naguib M. Activation of the CB2 receptor system reverses amyloid-induced memory deficiency. Neurobiol Ag. 2013;34:791–804.
39. Zhang HY, Gao M, Liu QR, Bi GH, Li X, Gardner EL, Wu J, Xi ZX. Cannabinoid CB2 receptors modulate midbrain dopamine neuronal activity and dopamine-related behavior in mice. Proc Natl Acad Sci U S A. 2014;111: E5007–15.
40. Zimmerman AM, Titishov N, Mechoulam R, Zimmerman S. Effect of stereospecific cannabinoids on the immune system. Adv Exp Med Biol. 1991;288:71–80.